2014 International Conference on Unmanned Aircraft Systems (ICUAS)
May 27-30, 2014. Orlando, FL, USA

Vector Field Guidance for Path Following and Arrival Angle Control

Seunghan Lim, Wooyoung Jung and Hyochoong Bang

***Abstract*—This paper focuses on unmanned aircraft guidance laws for a straight path and a circular orbit following using the vector field approach. The vector fields introduced in this paper can be applied to not only path following, but also other purposes such as arrival position, angle, and time control. Therefore, they could be applied to various missions providing advantages over other previous vector fields. Stability and performance of the path following has been proved and analyzed using the classical control theory. And simulation using a six degrees-of-freedom aircraft model shows that these guidance laws are effective for the missions even under the existence of wind disturbance.**

***Index Terms*—Vector field, vector field guidance, path following, trajectory tracking, arrival angle control, unmanned aircraft (UA), unmanned aerial vehicle (UAV).**

I. Introduction

UNMANNED aircraft(UA) have been considered to be one of the cost-effective approaches for target tracking, reconnaissance, and surveillance missions. Development costs and manufacturing efforts for UA are being reduced, whereas operational reliability is being increased. Therefore, UA are being applied to not only actual battle fields, but also civilian areas.

Typically, waypoints and paths are planned before UA are operated. Eun and Bang studied a cooperative task assignment and path planning approach for multiple UA [1]. They used the genetic algorithm to solve optimal problems. Moon *et al.* presented the hierarchical framework for task assignment and path planning in a dynamic environment [2]. Lim and Bang suggested strategies to establish waypoints for a surveillance mission using multiple UA [3].

After planning waypoints, paths are then planned by connecting each point together. When there are some constraints, the paths are planned by utilizing various geometric curves instead of straight lines. Chitsaz and LaValle used the Dubins path to generate time-optimal paths [4]. Shanmugavel *et al.* also employed the Dubins path to plan for cooperative missions [5]. Bézier curves are often introduced to satisfy an arrival angle to the waypoint [6, 7].

After planning paths, guidance laws are designed for path following. Park *et al.* demonstrated performance and stability for the nonlinear path following guidance method [8, 9]. Bhatia *et al.* designed a controller for commercial autopilots to track the Dubins path [10]. Kim and Kim proposed nonlinear guidance law combined with pseudo pursuit guidance [11]. Kaminer *et al.* presented a path following algorithm using L_1 adaptive augmentation for conventional autopilots [12].

The vector field approach is a well-known tool for guidance problems. This concept has been applied to different types of vehicles, such as wheeled, underwater, and aerial vehicles. Frew *et al.* presented a control structure for the standoff target tracking problem using cooperative fixed-wing aircraft [13]. They proved stable convergence to a circular orbit using Lyapunov stability theory. Gonçalves *et al.* presents a time-varying vector field based approach [14]. Frew suggested a scheme to operate cooperative vehicles with range and bearing sensors [15]. The mission was tracking an uncertain moving target. The algorithm they introduced transforms a vector field for a circular orbit into an ellipsoidal orbit. Summers and Akella also studied target tracking using a vector field, and they further developed the Lyapunov guidance vector field [16]. They considered an unknown moving target motion and wind, and established information architectures modeled by rigid graph theory. Zhu and Wang dealt with the problem of tracking an adversarial target using a vector field [17]. Lawrence *et al.* also designed a vector field for a circular orbit [18, 19]. They were defined in three dimensions, and the degree of attraction force could be controlled by a guidance parameter.

Lei *et al.* designed a vector field for path following in the Polar Regions using a small UA [20]. They focused on wind disturbance due to the wild environment of the Polar Regions; therefore, they used concepts of a vector field and sliding mode control simultaneously to increase the path following performance. Degen *et al.* extended the concept of a vector field into a tensor field [21]. Typical vector field guidance doesn't consider arrival time; however, they included time information in a vector field to satisfy an arrival time constraint with the dimension extended. Nelson *et al.* developed a path following based upon a concept of a vector

S. Lim is a senior researcher of Division of Aerospace Engineering, School of Mechanical, Aerospace and Systems Engineering, KAIST, Daejeon, South Korea (e-mail: shlim@ascl.kaist.ac.kr).

W. Jung is a Ph.D. candidate of Division of Aerospace Engineering, School of Mechanical, Aerospace and Systems Engineering, KAIST, Daejeon, South Korea (phone: +82-42-350-5796; e-mail: wyjung@ascl.kaist.ac.kr).

H. Bang is a professor of Division of Aerospace Engineering, School of Mechanical, Aerospace and Systems Engineering, KAIST, Daejeon, South Korea (e-mail: hcbang@ascl.kaist.ac.kr).

field [22]. They suggested two kinds of vector field guidance. One was for a straight path following, and the other one was for a circular orbit following. They generated course commands using a vector field; proved stability based upon sliding mode control; and introduced three types of combinations for path planning. The algorithms were verified by real flight tests. Meenakshisundaram *et al.* also designed a vector field for path following, however, one major difference was that it was designed in three dimensions [23].

This paper focuses on path following using the existing vector field approaches of [7, 24]. In fact, many vector fields have already been released for path following problems; however, the vector fields studied recently by Lim and Bang were shown to satisfy more constraints, such as arrival angle, and time. In this paper, path following strategies using the vector fields are suggested with analysis of performance. Then, the vector field can be applied, not only for path following, but also for surveillance, simultaneous attack, etc. Therefore, a software structure becomes simple, and serviceability for design and operation is improved, even if UA are engaged in complex missions.

II. Problem Description

This paper considers guidance laws for UA flying at constant altitude; therefore, a simple dynamic model is used as below.

$$\begin{aligned} \dot{x} &= v\cos\chi \\ \dot{y} &= v\sin\chi \\ \dot{v} &= -\left(v - v_d\right)/\tau_s \\ \dot{\chi} &= -\left\langle \chi - \chi_d \right\rangle/\tau_\chi \end{aligned} \tag{1}$$

where v and χ are ground speed and course, respectively, while x and y axes indicate north and east, respectively. $\langle a \rangle$ represents a function which wraps a to the interval $[-\pi, \pi]$. The maximum absolute value of $\mathrm{d}v/\mathrm{d}t$ and $\mathrm{d}\chi/\mathrm{d}t$ are restricted to 3m/s^2 and 30deg/s, respectively. The subscript d means a desired value, which should be tracked. τ_s and τ_χ represent time constants. The geometric relationships are defined in Fig.1. Equation (1) includes kinematics of an aircraft relative to airflow, and wind relative to the inertial coordinate frame. The vector fields in this research are designed to generate ground speed and course commands.

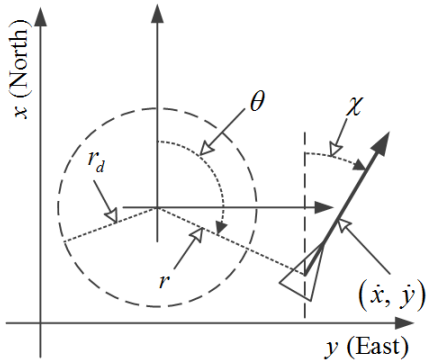

Fig.1 Geometric relations.

Hence, the associated controller should be designed for the purpose of tracking desired trajectories.

A vector field is constructed to achieve specific purposes. It is designed to generate vectors around a path to allow the UA to follow it. Vectors imply magnitude and direction, and they are used for ground speed and course commands. In the next section, basics of the vector field approach are introduced, which will be used for the guidance laws of UA in this study.

III. Vector Field Guidance

Three vector fields and their characteristics are addressed in this section. The two of them were already proposed in [7, 24]. They were designed to control arrival angle and time; however, they are employed for a different purpose in this research, that is, path following. The other vector field is newly proposed for the same purpose.

The first vector field is defined as follows [7]:

$$\begin{bmatrix} \dot{r} \\ r\dot{\theta} \end{bmatrix} = \frac{v_d}{r\sqrt{1+p_o^2 r^2}} \begin{bmatrix} -r \\ p_o r^2 \end{bmatrix} \tag{2}$$

where p_o is a parameter, which determines the configuration of the field, and the magnitude of (2) is always equal to v_d. The sign of p_o determines the direction of circular motion. The positive and negative parameters generate clockwise and counterclockwise vectors, respectively. And, the absolute value of p_o determines the degree of approaching velocity to the origin. Fig.2 shows examples of the vector field in (2). The bold lines represent the path of a particle on the field when it follows the vectors exactly.

An UA may be guided to satisfy the constraint of the arrival angle by using the vector field in (2). A corresponding parameter should be determined to satisfy the constraint, and it can be derived by using the chain rule as

$$p_o = -\frac{\left\langle \theta - \theta_t \right\rangle}{r} \tag{3}$$

Where θ_t is a desired arrival angle with regard to polar coordinates, of which the origin is a waypoint. The arrival time can be controlled, since the length of the path can be computed analytically. When constant speed is assumed, the desired speed is determined as

$$v_d = \left. \frac{-p_o r\sqrt{1+p_o^2 r^2} - \sinh^{-1}\left(p_o r\right)}{2p_o t_r} \right|_r^0 \tag{4}$$

where t_r is the remaining time until the desired arrival time [7].

The second vector field is defined as follows [22]:

$$\begin{bmatrix} \dot{r} \\ r\dot{\theta} \end{bmatrix} = \frac{v_d}{\sqrt{r^4 + \left(p_l^2 - 2\right) r_d^2 r^2 + r_d^4}} \begin{bmatrix} -\left(r^2 - r_d^2\right) \\ p_l^2 r_d r \end{bmatrix} \tag{5}$$

where p_l determines the configuration of the field, and the magnitude of (5) is equal to v_d. The positive and negative parameters generate clockwise and counterclockwise vectors around the origin, and the absolute value of p_l determines the degree of approaching velocity to the loitering circle, for which the radius is r_d. Fig.3 shows examples of the vector field.

Equation (5) is the same as the Frew *et al.*'s vector field of [13] when p_l is equal to 2. The bold lines represent the path of the particle of the field.

The arrival position outside the loitering circle can be controlled by using (5). If the desired arrival position is represented relative to the origin of the loitering circle, the appropriate parameter is determined such that

$$p_l = -\frac{2\langle \theta - \theta_t \rangle}{\mathrm{g}(r, r_d) - \mathrm{g}(r_t, r_d)} \tag{6}$$

where $r > r_t > r_d$, (r_t, θ_t) represents the desired arrival position, and the function $\mathrm{g}(a,b)$ is defined as

$$\mathrm{g}(a,b) \equiv \ln(a-b) - \ln(a+b). \tag{7}$$

And speed command is generated to control the arrival time as

$$v_d = -\frac{1}{t_r}\int_r^{r_t} \sqrt{1 + \left\{ (p_l r_d r) \Big/ \left(r^2 - r_d^2\right) \right\}^2}\, \mathrm{d}r. \tag{8}$$

The above equation cannot be solved analytically; therefore, the desired speed is computed numerically. This vector field has been designed to make an UA capture a target simultaneously [24].

The second vector field is useful to reconnoiter or track a target. However, it is difficult, due to the nonlinearity of (5), to analyze the performance of a circular orbit following when a dynamic model includes a time-delay. Therefore, we suggest another vector field to follow a circular orbit.

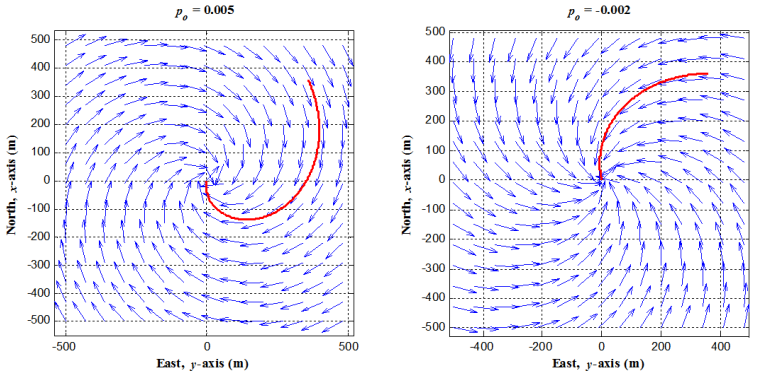

Fig.2 Examples of the vector field in (2).

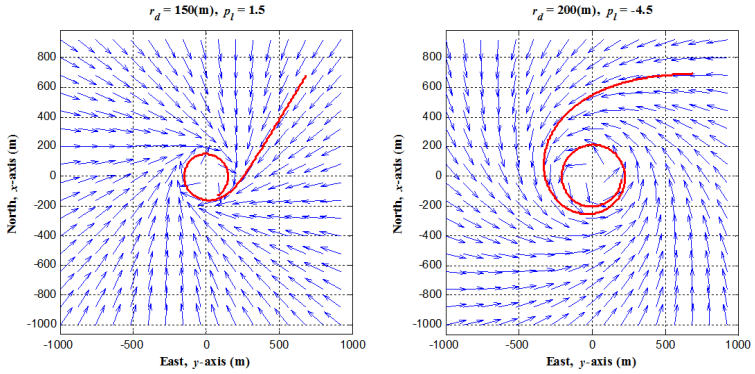

Fig.3 Examples of the vector field in (5).

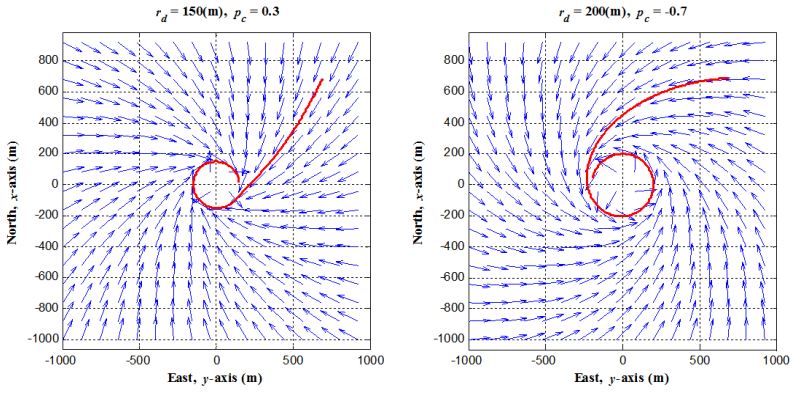

Fig.4 Examples of the vector field in (9).

$$\begin{bmatrix} \dot{r} \\ r\dot{\theta} \end{bmatrix} = \frac{v_d}{\sqrt{(r-r_d)^2 + p_c^2 r^2}} \begin{bmatrix} -(r-r_d) \\ p_c r \end{bmatrix} \tag{9}$$

The magnitude of the above vector is always v_d. It is worthwhile noting that p_c also determines the configuration of the field, and positive and negative parameters generate clockwise and counterclockwise vectors around the origin, respectively. A particle on the field with the smaller $|p_c|$ is pulled more toward the loitering circle, for which the radius is r_d. Fig.4 shows examples of the vector field. The bold lines represent the path of the particle. Arrival position can be also controlled when the proposed field is applied.

The vector field in (9) guides a particle to the desired position with the following guidance parameter.

$$p_c = -\frac{\langle \theta - \theta_t \rangle}{\ln(r-r_d) - \ln(r_t - r_d)} \tag{10}$$

where $r > r_t > r_d$. One can derive $\mathrm{d}r/\mathrm{d}t$ and $\mathrm{d}\theta/\mathrm{d}t$ from (9), then $\mathrm{d}r/\mathrm{d}\theta$ can be computed by the chain rule. After integration, the guidance parameter p_c is computed. If a particle on the field follows the vectors exactly, p_c remains constant until it arrives at the desired position. Using this assumption, the length of the path can be computed from $\mathrm{d}r/\mathrm{d}t$ as

$$l_c = \int_0^{t_r} v_d \,\mathrm{d}t = -\int_r^{r_t} \frac{\sqrt{(r-r_d)^2 + p_c^2 r^2}}{r - r_d} \mathrm{d}r \tag{11}$$

where l_c is the length of the remaining path. If t_r is given and assumed to have constant speed, then the desired speed is

$$v_d = -\frac{1}{t_r} \int_r^{r_t} \frac{\sqrt{(r-r_d)^2 + p_c^2 r^2}}{r - r_d} \mathrm{d}r \,. \tag{12}$$

The course commands are generated based on the vector fields, and they are

$$\chi_d = \theta + \operatorname{atan2}(r\dot{\theta}, \dot{r}) \,. \tag{13}$$

For the vector fields above, each time derivative of (13) could be derived analytically, so that it could be applied to improve the performance of course command tracking. In the following section, we propose how to determine the guidance parameters of the vector fields in (2) and (9) for path following.

IV. Path Following using Vector Field Guidance

In this section, we analyze the performance of path following with the vector fields introduced in the preceding sections. Most paths for a waypoint flight are planned by combinations of straight and circular segments. The vector fields (2) and (9) are a straight path and circular orbit following, respectively. The methods are introduced in the following subsection A and B, respectively.

A. Straight Path Following

An UA can follow a straight path based upon (2) when the vector field parameter is determined by

$$p_o = K_o \langle \theta - \theta_t \rangle \tag{14}$$

where K_o is a negative parameter, and it plays the role of a proportional gain to eliminate error from the straight path. The angles of the above equation are defined with regard to polar coordinates, of which the origin is on the following waypoint. θ is the angular position of the UA, and θ_t is the angle of the straight path. It is well described in Fig.5.

The vector field in (2) is linearized to prove the guidance stability and analyze the tracking characteristics. Without loss of generality, the desired straight path can be assumed as a path from the north to the south, that is, θ_t is 0. And the coordinates can be approximated when the angular error is small enough, that is, $|\theta| \ll 1$.

$$\begin{aligned} x &\approx r \\ y &\approx r\theta \end{aligned} \tag{15}$$

Therefore, (2) is approximated as

$$\dot{x} \approx \frac{-v}{\sqrt{1+(K_o y)^2}}, \qquad \dot{y} \approx \frac{vK_o y}{\sqrt{1+(K_o y)^2}} \tag{16}$$

when $p_o = K_o \theta$. Then the partial derivative of (16) with respect to y is

$$\frac{\partial \dot{y}}{\partial y} = \frac{vK_o\sqrt{1+(K_o y)^2} + \dfrac{vK_o y}{2\sqrt{1+(K_o y)^2}} + 2vK_o^3 y^2}{1+(K_o y)^2} \,. \tag{17}$$

Hence, (16) is linearized around $y = 0$ such that

$$\dot{y} = vK_o y \,. \tag{18}$$

If $|K_o y| \ll 1$, the high-order terms of (16) can be eliminated; therefore, (18) could be considered reasonable. As it can be seen in the equation linearized above, if K_o is negative, y always converges to 0, which indicates a stable behavior. However, this conclusion cannot be guaranteed when the tracking dynamics includes a time-delay.

If there is a time-delay when an UA tracks $\mathrm{d}y_d/\mathrm{d}t$, the system model can be expressed as

$$\begin{bmatrix} \dot{y} \\ \ddot{y} \end{bmatrix} = \begin{bmatrix} 0 & 1 \\ 0 & -\dfrac{1}{\tau_y} \end{bmatrix} \begin{bmatrix} y \\ \dot{y} \end{bmatrix} + \begin{bmatrix} 0 \\ \dfrac{1}{\tau_y} \end{bmatrix} \dot{y}_d \tag{19}$$

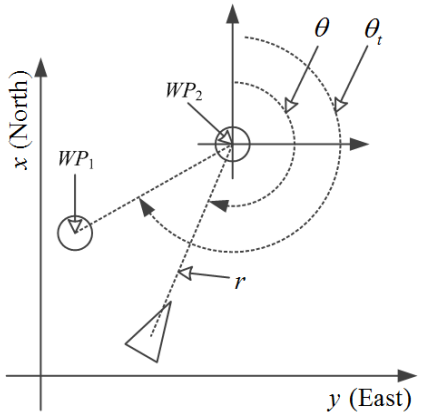

Fig.5 Geometric relations.

where τ_y is a time constant. When (18) is employed as the guidance command, then the model is expressed as follows:

$$\begin{bmatrix} \dot{y} \\ \ddot{y} \end{bmatrix} = \begin{bmatrix} 0 & 1 \\ \dfrac{vK_o}{\tau_y} & -\dfrac{1}{\tau_y} \end{bmatrix} \begin{bmatrix} y \\ \dot{y} \end{bmatrix}. \tag{20}$$

The characteristic equation of the above model is

$$s^2 + \frac{1}{\tau_y} s + \frac{-vK_o}{\tau_y} = 0 \tag{21}$$

where s is a Laplace transformation variable. Hence, the desired damping ratio and the natural frequency are

$$\zeta_o = \frac{1}{2\omega_o \tau_y}, \qquad \omega_o = \sqrt{\frac{-vK_o}{\tau_y}} \tag{22}$$

where ζ_o and ω_o are the damping ratio and the natural frequency of the straight path following dynamics. We can guess the path following performance with regard to K_o using (22) when τ_y is known. τ_y is approximately equal to τ_χ when the speed is not too fast. τ_χ depends on the performance of the controller to track a course command. If an UA is commanded to follow a straight path smoothly, then the desired damping ratio could be set to 1. Consequently, K_o is decided to be -0.02 by (22) with ζ_o =1, τ_y =0.5(sec), and v=25(m/sec). Fig.6 shows examples of the straight path following using (2) and (14).

B. Circular Orbit Following

If $p_c \neq 0$, the vector field in (9) always converges to a loitering circle. Therefore, any values except for p_c=0 can be used. However, if the tracking dynamics include a time-delay, then the large absolute value of p_c cannot guarantee the stability of convergence. In this subsection, we introduce a method for deciding an appropriate p_c for circular orbit following with the desired performance.

If $r \approx r_d$, (9) can be approximated as

$$\dot{r} \approx \frac{-v(r - r_d)}{|p_c| r_d}, \qquad r\dot{\theta} \approx \mathrm{sgn}(p_c) v \tag{23}$$

where sgn(a) is a function which returns the sign of a. If $(r - r_d) \equiv y_c$, then

$$\dot{y}_c = \frac{-vy_c}{|p_c| r_d}. \tag{24}$$

As one can see in the above equation, y_c always converges to 0. However, if there is a time-delay when an UA tracks dy_d/dt, the system model becomes

$$\begin{bmatrix} \dot{y}_c \\ \ddot{y}_c \end{bmatrix} = \begin{bmatrix} 0 & 1 \\ 0 & -\dfrac{1}{\tau_r} \end{bmatrix} \begin{bmatrix} y_c \\ \dot{y}_c \end{bmatrix} + \begin{bmatrix} 0 \\ \dfrac{1}{\tau_r} \end{bmatrix} \dot{y}_d \tag{25}$$

where τ_γ is a time constant. When (24) is used as the guidance command, then the above model can be rewritten as

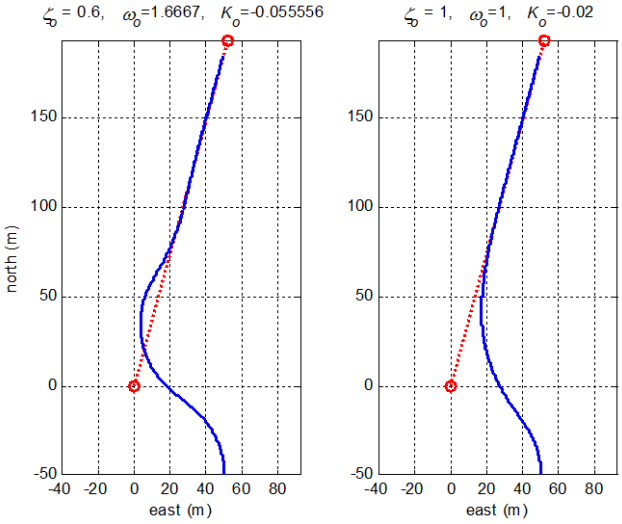

Fig.6 Position trajectories of a straight path following with τ_χ = 0.5, and v=25(m/sec).

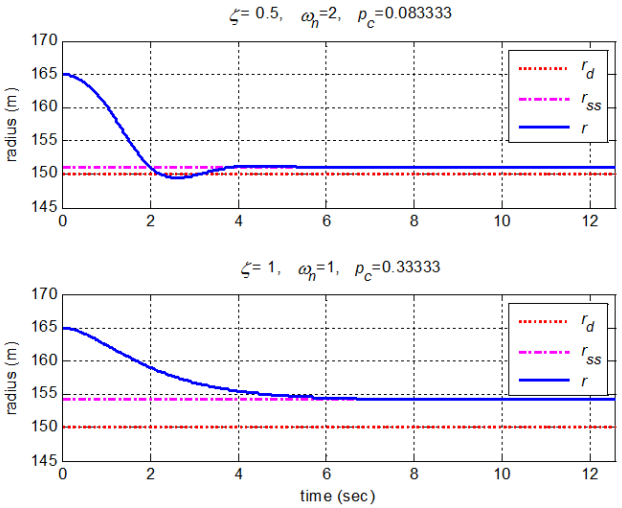

Fig.7 Radius trajectories of a circular orbit following with τ_χ=0.5, v=25(m/sec), and r_d=150(m).

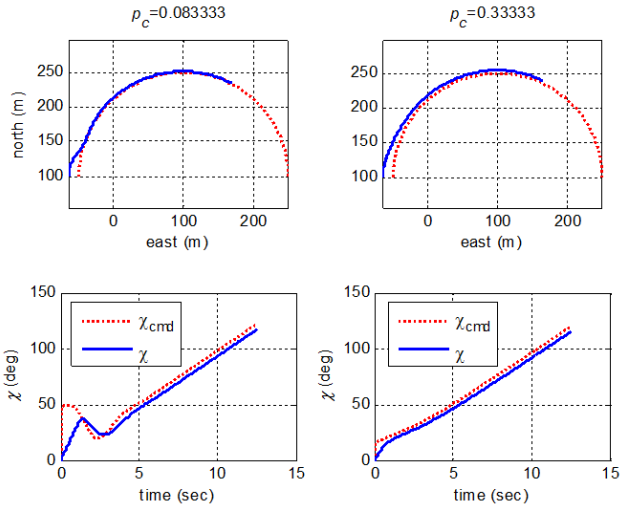

Fig.8 Position and course trajectories of a circular orbit following with τ_χ=0.5, v=25(m/sec), and r_d=150(m).

$$\begin{bmatrix} \dot{y}_c \\ \ddot{y}_c \end{bmatrix} = \begin{bmatrix} 0 & 1 \\ \dfrac{-v}{|p_c| r_d \tau_r} & -\dfrac{1}{\tau_r} \end{bmatrix} \begin{bmatrix} y_c \\ \dot{y}_c \end{bmatrix}. \quad (26)$$

Then, the characteristic equation of the above model is given by

$$s^2 + \frac{1}{\tau_r} s + \frac{v}{|p_c| r_d \tau_r} = 0. \quad (27)$$

Hence, we can get the damping ratio and the natural frequency.

$$\zeta_c = \frac{1}{2\omega_c \tau_r}, \qquad \omega_c = \sqrt{\frac{v}{|p_c| r_d \tau_r}} \quad (28)$$

where ζ_c and ω_c are the damping ratio and the natural frequency of a circular orbit following. One can guess the performance of circular orbit following with regard to p_c using (28) when τ_r is known. τ_r is approximately equal to τ_χ when the speed is not too fast. If an UA should track a circular orbit asymptotically, then the desired damping ratio is equal to 1. Consequently, p_c is selected to be 0.33 by (28) with ζ_c=1, τ_r=0.5(sec), and v=25(m/sec). Figs.7 and 8 show examples of circular orbit following using (9).

At this point, it is necessary to address the steady-state error issue. When an UA follows the vector field in (5) or (9) exactly, it always converges to the desired loitering circle asymptotically. However, it should be noted that steady-state error exists when the tracking dynamics include a time-delay, as in Figs.7 and 8. The error is issued because of a continuously varying course command. When $r \geq r_d$, the time derivative of the desired course satisfies

$$0 < |\dot{\chi}_d| \leq \frac{v}{r_d}, \quad (29)$$

Therefore, the steady-state error of the system becomes

$$0 < \lim_{t \to \infty} |\chi - \chi_d| \leq \frac{v}{r_d} \tau_\chi, \quad (30)$$

where the command input for the circular orbit following can be assumed to be a ramp function when $r \approx r_d$. Equation (30) shows that the steady-state error of the radius always exists.

When the UA is close to a specific circular orbit, for which the radius is greater than r_d, the time derivative of the course command is approximately equal to the derivative of the desired circular orbit, that is, v/r_d. Therefore, the below relationship can be established from (1) and (30) such that

$$\frac{-(\chi - \chi_d)}{\tau_\chi} = \dot{\chi} \approx \dot{\chi}_d \approx \frac{v}{r_d}. \quad (31)$$

Without loss of generality, we can assume that the UA approaches a specific circular orbit, and the radius of the orbit is r_{ss} and the angular position of the UA is 0. Note that r_{ss} is always greater than r_d due to a steady-state error of the course. Since the UA is close to the orbit and the angular position is 0, the course and the command at this point become $\pi/2$ and

$$\chi_d = \theta + \text{atan}\,2\left(r\dot{\theta}, \dot{r}\right) = \text{atan}\,2\left(p_c r_{ss}, -(r_{ss} - r_d)\right), \quad (32)$$

respectively. The above equation is determined by (9) with the function atan2(y, x) is the fourth quadrant arctangent function, and atan2(y, x) $\in [-\pi, \pi]$. After substituting (32) into (31), then

$$r_{ss} \approx \frac{\tan\left(v_d \tau_\chi / r_d + \pi/2\right)}{p_c + \tan\left(v_d \tau_\chi / r_d + \pi/2\right)} r_d. \quad (33)$$

One can see the estimation results of the radius of the orbit in Fig.7, and verify that the results are well predicted.

V. Strategies for Waypoint Flight

Using the methods in the preceding section, strategies for a waypoint flight are suggested in this section. After planning waypoints, paths are planned by combinations of straight and circular segments in most cases. Nelson *et al.* suggested the combinations in [21]. Three types were proposed, and their purposes were to preserve equal path lengths, for flying through the waypoints, and minimizing the path lengths. We consider just one case in this study, that is, flying through the waypoints. As mentioned in section II, the UA is under dynamic constraints. The maximum absolute value of dv/dt and dχ/dt are restricted to 3m/s^2 and 30deg/s, respectively.

A. Straight Path Following

In this subsection, the case of flying through the waypoints using only a straight path following is analyzed. There are two simulation results in Fig.9. In these simulations, only the vector field of (2) is used. In the simulation #1 and #2, each simulation contains two straight paths with contained angles 15deg and 135deg, respectively. The speed of the UA is 25m/s, the time constant is 0.5, and the desired damping ratio is 0.707.

B. Straight Path Following and Arrival Angle Control

In this subsection, flying through the waypoints using a straight path following and arrival angle control approaches is analyzed. Let us define some geometric relations first defined

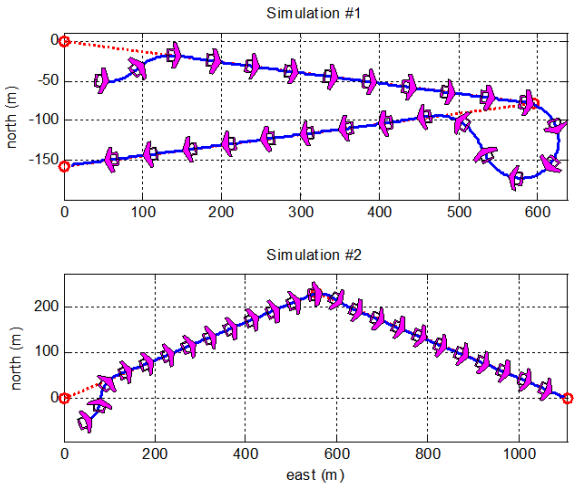

Fig.9 Path following simulation results for a straight path following.

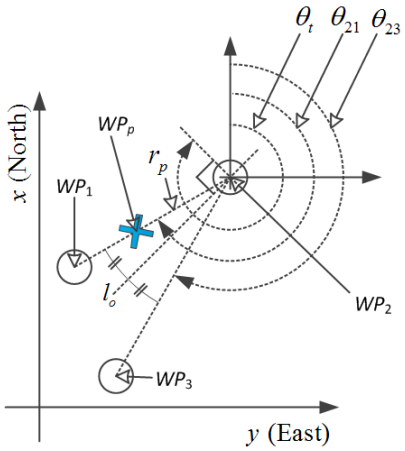

Fig.10 Geometric relations.

in Fig.10. The WP_p is a point, where the UA changes guidance mode from straight path following to arrival angle control. r_p is the distance from WP_2 to WP_p. l_o is a bisector, which divides the interior angle between two lines equally. Of the two lines, one connects WP_1 and WP_2, and the other connects WP_2 and WP_3. θ_t denotes the angle of the line perpendicular to l_o. The first guidance mode applied is given by (2), and the parameter p_o is determined by (14) before the UA arrives at WP_p. After arrival, p_o is determined by (3) to control the arrival angle, θ_t. If the UA arrives at WP_2, then the origin of polar coordinates is changed to WP_3, while p_o is determined by (14) again.

To control the arrival angle, an appropriate r_p is required. As someone can guess, the UA cannot arrive at WP_2 if r_p is too small due to a dynamic constraint. The distance could be determined based on analysis about the curvature of a path. The curvature of the path is

$$|\kappa_o| = \frac{r^2 + 2\left(\frac{dr}{d\theta}\right)^2 - r\frac{d^2 r}{d\theta^2}}{\left(r^2 + \left(\frac{dr}{d\theta}\right)^2\right)^{3/2}}. \tag{34}$$

Hence, the curvature of (2) can be derived as

$$|\kappa_o| = \frac{p_o\left(2 + r^2 {p_o}^2\right)}{\left(1 + {p_o}^2 r^2\right)^{3/2}}. \tag{35}$$

And derivative of the curvature with regard to r is

$$\frac{d|\kappa_o|}{dr} = -\frac{{p_o}^4 r\left({p_o}^2 r^2 + 4\right)\sqrt{\frac{1}{{p_o}^2} + r^2}}{\left({p_o}^2 r^2 + 1\right)^3} \le 0. \tag{36}$$

This equation implies that the maximum curvature of the path occurs at $r = 0$. Therefore,

$$\max_r |\kappa_o(r)| = |\kappa_o(0)| = |2p_o|. \tag{37}$$

If the UA is on the path and the desired arrival angle is θ_t, then the maximum curvature predicted is

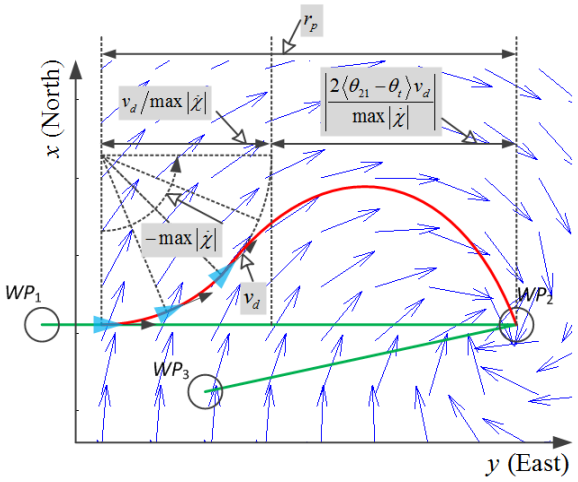

Fig.11 Introduction how to determine r_p.

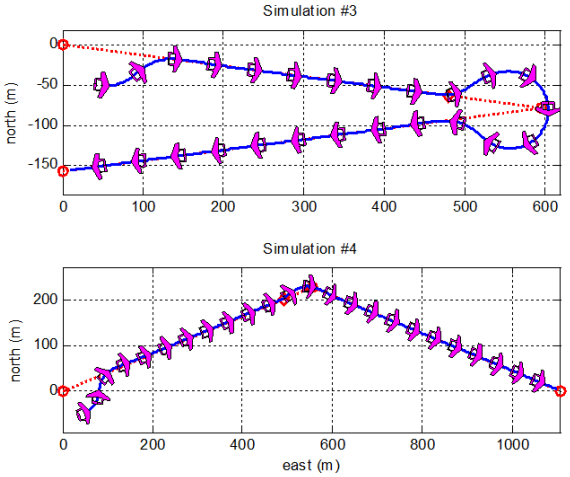

Fig.12 Path following simulation results for a straight path following and arrival angle control.

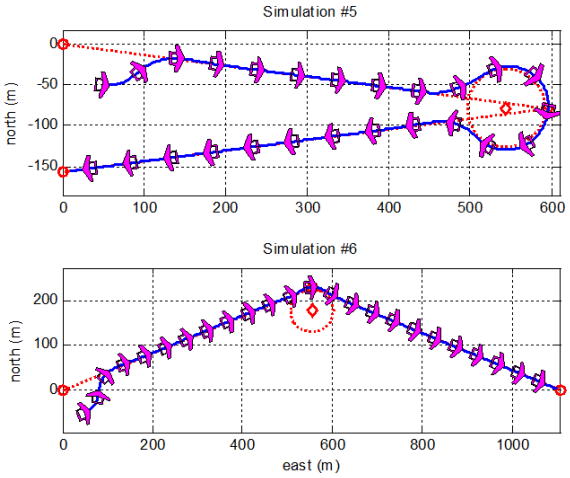

Fig.13 Path following simulation results for a straight path and a circular orbit following.

$$\max_r |\kappa_o| = \left| 2\frac{\langle \theta_{21} - \theta_t \rangle}{r_p} \right| \tag{38}$$

which should be less than the turning rate capability of the UA.

$$\max_r |\kappa_o| \le \frac{\max|\dot{\chi}|}{v}. \tag{39}$$

If not, the UA cannot follow the vector field, and then it cannot reach WP_2. Let us note that v can be substituted by v_d, since the UA can be assumed to track the speed command sufficiently well. Therefore,

$$\left| \frac{2\langle \theta_{21} - \theta_t \rangle v_d}{\max|\dot{\chi}|} \right| \le r_p. \tag{40}$$

Moreover, when the equation determining p_o is changed from (14) to (3), the course command is changed discontinuously. Hence, the UA cannot follow the command exactly at that moment. To allow enough time to track the command, the extra distance is added. We can guess that dr/dt is always smaller than 0 when $r > 0$ from (2). It implies that the vector field of (2) cannot generate vortex flow. Therefore, the difference between χ_d from (3) and (14) is always smaller than 90deg. Hence, the turning radius is added for extra distance as seen in Fig.. Therefore the appropriate r_p can be determined by

$$r_p = \left| \frac{2\langle \theta_{21} - \theta_t \rangle v_d}{\max|\dot{\chi}|} \right| + \frac{v_d}{\max|\dot{\chi}|}. \tag{41}$$

The third and the fourth simulation results are shown in Fig.12. The angles between the first and the third waypoints are 15deg and 135deg, respectively. The speed of the UA is 25m/s, the time constant is 0.5, and the desired damping ratio is 0.707. As in the results, the UA does not fly through WP_2 exactly, since the tracking dynamics are subject to a time constant. However, the amount of error is within a permissible range.

C. Following Straight Path and Circular Orbit

In this subsection, flying through the waypoints using straight path and circular orbit following strategies is analyzed. When the UA follows straight segments, (2) and (14) are used. When the UA approaches WP_2, then the vector field guidance is changed to (9). The center is on the bisector l_o, and is r_{ss}

TABLE I Configuration and inertia information of the 6-DoF aircraft model

WingArea	0.33m2	Wing Span	0.22m	Mean Chord	1.50m	-	-
Mass	2.8kg	I_{xx}	0.075kg·m2	I_{yy}	0.137kg·m2	I_{zz}	0.165kg·m2

TABLE II Aerodynamic coefficients of the 6-DoF aircraft model

C_{D_0}	0.070000	e	0.735500	C_{Y_β}	-0.284375	C_{l_β}	-0.156782	C_{n_β}	0.017482
C_{L_0}	0.157352	C_{m_0}	-0.028765	C_{Y_p}	-0.164212	C_{l_p}	-0.542617	C_{n_p}	-0.012460
C_{L_α}	4.936260	C_{m_α}	-0.691753	C_{Y_r}	-0.095064	C_{l_r}	0.130093	C_{n_r}	-0.067092
C_{L_q}	5.967029	C_{m_q}	-8.165052	$C_{Y_{\delta a}}$	0.111658	$C_{l_{\delta a}}$	0.263704	$C_{n_{\delta a}}$	0.011511
$C_{L_{\delta e}}$	0.216658	$C_{m_{\delta e}}$	-0.700510	$C_{Y_{\delta r}}$	0.070268	$C_{l_{\delta r}}$	0.004211	$C_{n_{\delta r}}$	-0.032286

TABLE III Flight scenario

Section	Coordinates (m)	hd (m)[1)]	vd (m/s)	Description for guidance mode
~ WP1	(300, -100)	150	22	Arrival angle control, θ_t = 198deg.
~ WP2	(600, 0)	150	22	Following the straight line. ζ_o = 0.9.
~ WP3	(800, 300)	150	22	Following the straight line. ζ_o = 0.9.
~ WP4	(400, 400)	150	22	Following the straight line. ζ_o = 0.9.
~ WP5	(300, 700)	150	22	Arrival angle control, θ_t = 225deg.
~ WP6	(600, 1000)	150	22	Following the straight line. ζ_o = 0.9.
~ WP7	(400, 1200)	150	22	Arrival angle control, θ_t = 0deg.
~ WP8	(0, 1200)	150	22	Following the straight line. ζ_o = 0.9.
~ WP9	(-200, -500)	250	22	Following the circular orbit. rd = 150m. ζ_c = 1.5.
~ WP10	(-300, -100)	150	22	Following the straight line. ζ_o = 0.9.

1) Altitude command

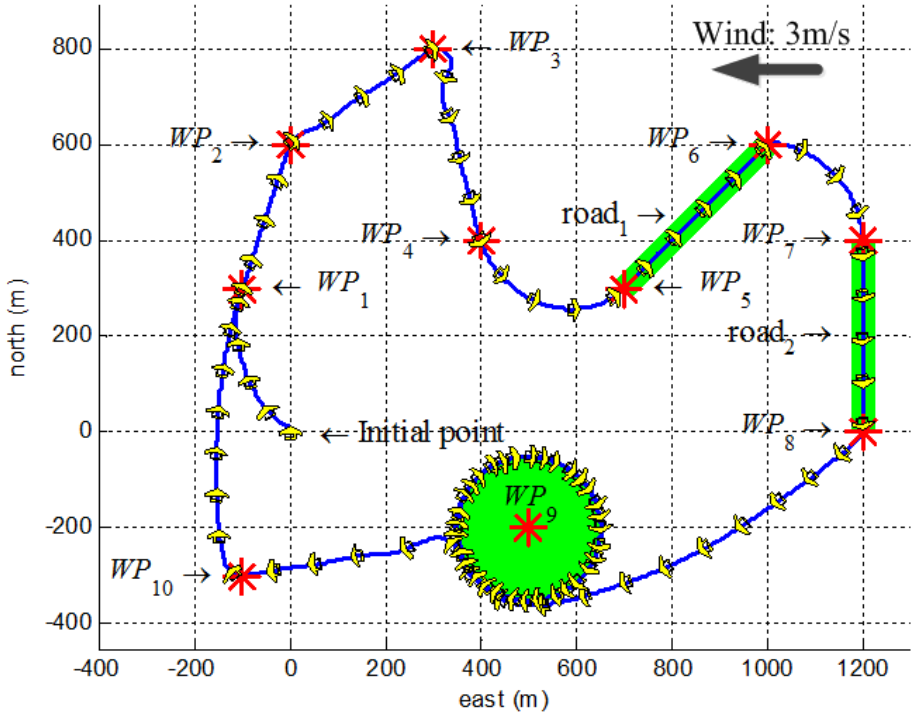

Fig.14 Waypoint flight simulation results using 6-DoF aircraft model with constant wind.

away from WP_2. The fifth and the sixth simulation results are shown in Fig.13. The angles between the first and the third waypoints are 15deg and 135deg, respectively. The speed of the aircraft is 25m/s, the time constant is 0.5, ζ_o and ζ_c are 0.707 and 0.5, respectively.

D. Simulation 6-DoF Non-linear Aircraft Model

The previous simulations used the simple time-delay model of (1). However, the six degree-of-freedom aircraft model is used with constant wind in this subsection. All aerodynamic coefficients are computed using AVL [25]. The information on the aircraft model is shown in TABLE I and TABLE II. With the information, forces and moments can be computed, and applied to 6-DoF nonlinear dynamic equations of motion. Detailed equations are shown in [26]. PID controllers are designed to track guidance commands generated by the vector fields.

A summary of the flight scenario is shown in TABLE III. We assume that there are roads, which connect WP_5 to WP_6 and WP_7 to WP_8, and which need to be observed. When the UA observes roads, stable attitude might improve the surveillance performance; therefore, the arrival angles are controlled to approach the beginning of the roads with stable attitude. As it can be seen in the trajectory around WP_3 of Fig.14, there is a period, over which the trajectory is oscillated. However, one can also recognize that oscillations are not occurring around WP_5 and WP_7, since the arrival angles are controlled; therefore, a rapid maneuver is not required. It is assumed that a stationary target is located on WP_9, and the UA rotates around the target for surveillance. The rest of the sections are waypoint flight; therefore the UA follows the straight lines. The wind blows at a speed of 3m/s, and the direction of the wind is 90deg. The simulation result is shown in Fig.14. It shows that the vector field guidance proposed in this paper is useful enough when it is implemented onboard.

VI. Conclusion

In this paper, the guidance laws for a path following flight and the strategies for a waypoint flight are introduced by using the vector field approach. Contributions of this paper can be summarized as follows. 1) The traditional vector field for straight path following is extended to control arrival angle. The guidance parameter can be determined if one knows the time-delay of the controller and the damping ratio for path following scenario. 2) Vector fields to follow a straight path have been already developed. However, the vector field of this paper could be applied to not only path following but also arrival angle and time control without any path planning algorithms; therefore, the UA can engage in various missions with a simple software structure. 3) Earlier studies have used the vector field method to follow a circular orbit. The associated stability has been proved only for the convergence to the orbit. However, the vector field for a circular orbit in this study not only could verify stability, but also desired path following performance can be satisfied. All of these contributions are demonstrated by the simulations with 6-DoF nonlinear dynamic equations of motion.

REFERENCES

[1] Y. Eun and H. Bang, "Cooperative Task Assignment/Path Planning of Multiple Unmanned Aerial Vehicles using Genetic Algorithms," *Journal of aircraft,* vol. 46, p. 338, 2009.

[2] S. Moon, E. Oh, and D. H. Shim, "An Integral Framework of Task Assignment and Path Planning for Multiple Unmanned Aerial Vehicles in Dynamic Environments," *Journal of Intelligent & Robotic Systems,* pp. 1-11, 2012.

[3] S. Lim and H. Bang, "Waypoint Planning Algorithm using Cost Functions for Surveillance," *International Journal of Aeronautical and Space Science,* vol. 11, pp. 136-144, 2010.

[4] H. Chitsaz and S. M. LaValle, "Time-optimal Paths for a Dubins Airplane," in *IEEE Conference on Decision and Control*, 2007, pp. 2379-2384.

[5] M. Shanmugavel, A. Tsourdos, B. White, and R. Zbikowski, "Co-operative path planning of multiple UAVs using Dubins paths with clothoid arcs," *Control Engineering Practice,* vol. 18, pp. 1084-1092, Sep 2010.

[6] M. Shanmugavel, A. Tsourdos, R. Zbikowski, B. A. White, C. A. Rabbath, and N. Lechevin, "A Solution to Simultaneous Arrival of Multiple UAVs using Pythagorean Hodograph Curves," in *American Control Conference*, Minneapolis, MN, USA, 2006, pp. 2813-2818.

[7] S. Lim and H. Bang, "UAV Guidance Laws to Arrival at Desired Position and Time from Desired Direction," presented at the International Conference on Control, Automation and Systems, KINTEX, Gyeonggi-do, Korea, 2011.

[8] S. Park, J. Deyst, and J. P. How, "A New Nonlinear Guidance Logic for Trajectory Tracking," presented at the AIAA Guidance, Navigation, and Control Conference, 2004.

[9] S. Park, J. Deyst, and J. P. How, "Performance and Lyapunov Stability of a Nonlinear Path-following Guidance Method," *Journal of Guidance, Control, and Dynamics,* vol. 30, pp. 1718-1728, Nov-Dec 2007.

[10] A. Bhatia, E. Frazzoli, M. Graziano, S. Karaman, and R. Naldi, "Dubins Trajectory Tracking using Commercial Off-The-Shelf Autopilots," presented at the AIAA Guidance, Navigation, and Control Conference and Exhibit, Hawaii, USA, 2008.

[11] Mingu Kim and Youdan Kim, "Multiple UAVs nonlinear Guidance Laws for Stationary Target Observation," *International Journal of Aeronautical and Space Science,* vol. 14, pp. 67-74, 2013

[12] I. Kaminer, A. Pascoal, E. Xargay, N. Hovakimyan, C. Cao, and V. Dobrokhodov, "Path Following for Unmanned Aerial Vehicles using L1 Adaptive Augmentation of Commercial Autopilots," *Journal of Guidance, Control, and Dynamics,* vol. 33, pp. 550-564, 2010.

[13] E. W. Frew, D. A. Lawrence, and S. Morris, "Coordinated Standoff Tracking of Moving Targets using Lyapunov Guidance Vector Fields," *Journal of Guidance, Control, and Dynamics,* vol. 31, p. 17, Mar.-Apr. 2008.

[14] Gonçalves, V.M., Pimenta, L.C.A., Maia, C.A., Dutra, B.C.O., and Pereira, "Vector fields for robot navigation along time-varying curves in ndimensions." *IEEE Transactions on Robotics*, 26(4), 647–659. 2010.

[15] E. W. Frew, "Cooperative Standoff Tracking of Uncertain Moving Targets using Active Robot Networks," presented at the IEEE International Conference on Robotics and Automation, Roma, Italy, 2007.

[16] T. H. Summers, M. R. Akella, and M. J. Mears, "Coordinated Standoff Tracking of Moving Targets: Control Laws and Information Architectures," *Journal of Guidance, Control, and Dynamics,* vol. 32, p. 14, Jan.-Feb. 2009.

[17] S. Zhu and D. Wang, "Adversarial Ground Target Tracking Using UAVs with Input Constraints," *Journal of Intelligent & Robotic Systems,* vol. 65, pp. 521-532, 2012.

[18] D. A. Lawrence, "Lyapunov vector fields for UAV flock coordination," presented at the 2nd AIAA "Unmanned Unlimited" Systems, Technologies, and Operations - Aerospace, Land, and Sea Conference, Workshop and Exhibition, San Diego, CA, USA, 2003.

[19] D. A. Lawrence, E. W. Frew, and W. J. Pisano, "Lyapunov Vector Fields for Autonomous Unmanned Aircraft Flight Control," *Journal of Guidance, Control, and Dynamics,* vol. 31, p. 10, 2008.

[20] X. S. Lei, L. Bai, Y. H. Du, C. X. Miao, Y. Chen, and T. M. Wang, "A Small Unmanned Polar Research Aerial Vehicle based on the Composite Control Method," *Mechatronics,* vol. 21, pp. 821-830, Aug 2011.

[21] S. C. Degen, L. M. Alvarez, J. J. Ford, and R. A. Walker, "Tensor Field Guidance for Time-based Waypoint Arrival of UAVs by 4D Trajectory Generation," presented at the IEEE Aerospace Conference, Big Sky, Montana, USA, 2009.

[22] D. R. Nelson, D. B. Barber, T. W. McLain, and R. W. Beard, "Vector Field Path Following for Miniature Air Vehicles," *IEEE Transactions on Robotics,* vol. 23, pp. 519-529, 2007.

[23] V. Meenakshisundaram, V. Gundappa, and B. S. Kanth, "Vector field guidance for path following of MAVs in three dimensions for variable altitude maneuvers," *International Journal of Micro Air Vehicles,* vol. 2, pp. 255-265, 2010.

[24] S. Lim, Y. Kim, D. Lee, and H. Bang, "Standoff Target Tracking using a Vector Field for Multiple Unmanned Aircrafts," *Journal of Intelligent & Robotic Systems,* vol. 69, pp. 347-360, 2013.

[25] M. Drela and H. Youngren. (2011). *Athena Vortex Lattice*. Available: http://web.mit.edu/drela/Public/web/avl/

[26] B.L. Stevens and F. L. Lewis, Aircraft Control and Simulation" Wiley & sons, inc., 1992